Organic compounds on comet 67P/Churyumov-Gerasimenko revealed by COSAC mass spectrometry

Fred Goesmann, Helmut Rosenbauer, Jan Hendrik Bredehoft, Michel Cabane, Pascale Ehrenfreund, Thomas Gautier, Chaitanya Giri, Harald Krüger, Léna Le Roy, A. J. Macdermott, et al.

Organic compounds on comet 67P/Churyumov-Gerasimenko revealed by COSAC mass spectrometry

Fred Goesmann,[1*] Helmut Rosenbauer,[1] Jan Hendrik Bredehöft,[2] Michel Cabane,[3] Pascale Ehrenfreund,[4,5] Thomas Gautier,[6] Chaitanya Giri,[1,7] Harald Krüger,[1] Léna Le Roy,[8] Alexandra J. MacDermott,[9] Susan McKenna-Lawlor,[10] Uwe J. Meierhenrich,[7] Guillermo M. Muñoz Caro,[11] Francois Raulin,[12] Reinhard Roll,[1] Andrew Steele,[13] Harald Steininger,[1] Robert Sternberg,[12] Cyril Szopa,[3] Wolfram Thiemann,[2] Stephan Ulamec[14]

1. Max Planck Institute for Solar System Research, Justus von Liebig Weg 3, 37077 Göttingen, Germany.
2. University of Bremen, Institute for Applied and Physical Chemistry, Leobener Strasse NW2, 28359 Bremen, Germany.
3. Université Versailles St-Quentin, Sorbonne Universités, Université Pierre et Marie Curie Univ. Paris 06, Centre National de la Recherche Scientifique (CNRS)–Institut National des Sciences de l'Univers, Laboratoire Atmosphéres, Milieux, Observations Spatiales–Institut Pierre Simon Laplace (LATMOS-IPSL), 4 Place Jussieu 75005 Paris.
4. Leiden Observatory, Post Office Box 9513, 2300 RA Leiden, Netherlands.
5. Space Policy Institute, George Washington University, Washington, DC, USA.
6. Goddard Space Flight Center, Greenbelt, MD 20771, USA.
7. University Nice Sophia Antipolis, Institut de Chimie de Nice Unite Mixte de Recherche (UMR) 7272 CNRS, Avenue Valrose, 06108 Nice, France.
8. Center for Space and Habitability, University of Bern, Sidlerstrasse 5, CH-3012 Bern, Switzerland.
9. University of Houston–Clear Lake, 2700 Bay Area Boulevard, Houston, TX 77058, USA.
10. Space Technology Ireland, Ltd., Maynooth, Co. Kildare, Ireland.
11. Centro de Astrobiología, Instituto Nacional de Técnica Aeroespacial–Consejo Superior de Investigaciones Científicas, Ctra. de Ajalvir, km 4, Torrejón de Ardoz, 28850 Madrid, Spain.
12. Laboratoire Interuniversitaire des Systèmes Atmosphériques (LISA), UMR CNRS 7583, Université Paris-Est Créteil and Université Paris-Diderot, 94000 Créteil, France.
13. Geophysical Laboratory, Carnegie Institution of Washington, Washington, DC, USA.
14. German Aerospace Center, Deutsches Zentrum für Luft und Raumfahrt (DLR), 51147 Cologne, Germany.

*Corresponding author. E-mail: goesmann@mps.mpg.de

Comets harbor the most pristine material in our solar system in the form of ice, dust, silicates, and refractory organic material with some interstellar heritage. The evolved gas analyzer Cometary Sampling and Composition (COSAC) experiment aboard Rosetta's Philae lander was designed for in situ analysis of organic molecules on comet 67P/ Churyumov-Gerasimenko. Twenty-five minutes after Philae's initial comet touchdown, the COSAC mass spectrometer took a spectrum in sniffing mode, which displayed a suite of 16 organic compounds, including many nitrogen-bearing species but no sulfur-bearing species, and four compounds—methyl isocyanate, acetone, propionaldehyde, and acetamide—that had not previously been reported in comets.

The study of the chemical composition of comets provides key information about the raw materials present in the early solar system (1, 2). Ground and space-based observations have identified over 20 organic molecules in comet comae (3, 4), a subset of which are of prebiotic interest (5, 6).

The Cometary Sampling and Composition (COSAC) experiment on Rosetta's lander Philae was designed to detect and identify organic molecules in the material of comet 67P (7). It consists of a gas chromatograph (GC) and a time-of-flight mass spectrometer (TOF-MS) to analyze samples delivered by the sample drilling and distribution system (SD2). COSAC can also operate in sniffing mode, in which the MS accumulates data without active

sampling by SD2. Molecules that have passively entered the instrument are ionized, accelerated, and finally registered by COSAC. MS sniffings were made several times between launch and arrival at the comet, including during a fly-by of Lutetia (8). MS sniffings were made on arrival at 67P from 10 km above the surface, after initial touchdown, and at the final resting site (Fig. 1).

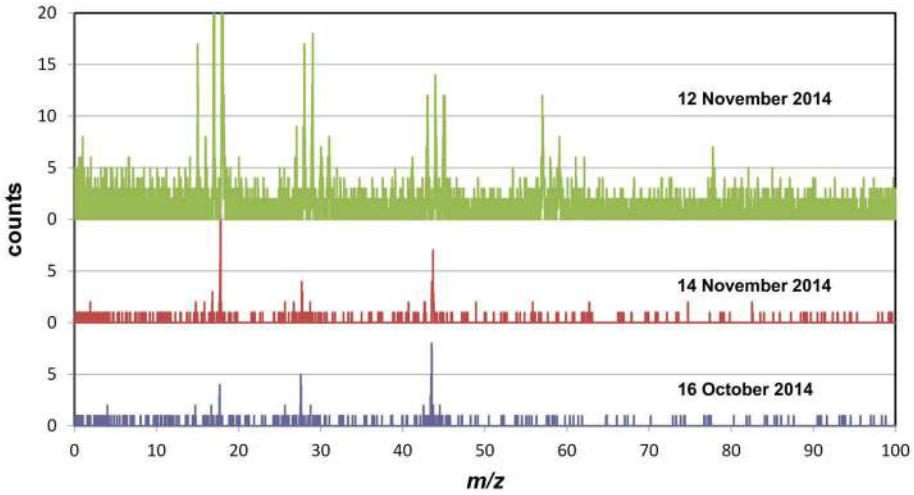

Figure 1. Mass spectra taken by COSAC in "sniffing mode." Top (green): spectrum taken 25 min after first touchdown; the m/z 18 peak reached a height of 330 counts, but the spectrum is truncated to show smaller peaks more clearly; middle (red): final spectrum, taken 2 days later at the current Philae position; bottom (blue): first spectrum, obtained in orbit 27 days before landing, from a distance of 10 km.

The Philae lander first touched down on 67P on 12 November 2014 at 15:34:04 UTC and then bounced. The impact excavated about 0.4 m3 of solid material (9), some of which would have entered COSAC's two exhaust pipes, which are on the bottom of the lander (10), and then stuck to the inside of the 2-cm-wide pipes. The temperature in these pipes was 12° to 15°C (10), midway between the cold cometary exterior and the heated interior of the lander, allowing volatile organics to sublime and be detected by the MS in a measurement that began at 16:00:30 UTC and ended at 16:02:50 UTC, when the lander was about 150m above the surface on its first bounce. We focus here on this spectrum (green in Fig. 1), which differs fundamentally in the number and intensity of its peaks from the undisturbed spectra taken before and after, and represents excavated cometary material (10). Our approach was to find the best fit to this spectrum of a superposition of standard National Institute of Standards and Technology (NIST) mass spectra (11) of candidate cometary molecules. The spectral deconvolution methodology used is similar to that used in other space missions [such as the Ion and Neutral Mass Spectrometer (INMS) measurements by Cassini and the GCMS on the Huygens probe] (12–14).

Because COSAC has a mass resolution of only 300, single mass peaks cannot be resolved into different molecular species [e.g., CO, N2, and C2H4, all at a mass/charge ratio (m/z) of 28, are indistinguishable]. Analysis (10) was limited to compounds below m/z 62 because signals beyond this value are too faint to be distinguished reliably from noise. The

peak at m/z 78, for example, is not real: Several ions coincidentally ended up in a single channel, leaving neighboring ones empty (10). All conceivable molecules were first listed and their fragmentation patterns evaluated (table S1). Elimination of molecules with incompatible fragmentation patterns (for reasons described in table S3) led to a short-list of candidate molecules (table S2). We further reduced the short list by making the fit in order of decreasing mass, starting from m/z 59 (10), and eliminating unstable and unsaturated species. This yielded a good fit to all peaks (except m/z 15 and a fraction of m/z 29, Fig. 2) with 16 species from several families of molecules—alcohols, carbonyls, amines, nitriles, amides, and isocyanates—in a consistent combination (Table 1). Peaks for m/z < 10 were not included in the fit because they are not listed in the standard NIST mass spectra (11). The molecular abundances of these compounds relative to that of water (Table 1) were corrected for electron cross section (table S4). The absence of ions at m/z 32 indicates a lack of sulfur-bearing species (Fig. 2 and Table 1). Amino acids were not included in the fit because the molecular ion peaks of glycine (m/z 75) and alanine (m/z 89) are negative after background subtraction, thereby suggesting that they are noise. Although fragment peaks assigned to glycine and alanine in the NIST standard spectra (11) are present in the COSAC spectrum (in the m/z 30s to 40s range), any contribution to these fragment peaks from amino acids is difficult to disentangle from the contributions of other species.

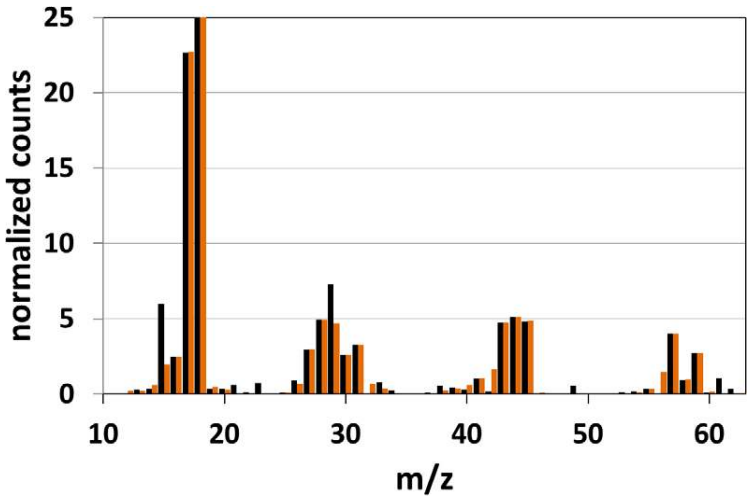

Figure 2. The fit to the observed spectrum. Comparison of the COSAC original mass spectrum (black bars for each integer mass) and the spectrum reconstructed from the best fit (orange bars to right of original signal). The peak heights are normalized to 100 for the m/z 18 peak (which has been truncated).

The main source of error is the low signal intensity, averaging about 100 counts (table S1). A statistical square-root of n approach yields a standard deviation of 10%. In addition, the NIST standard spectra (11) have a 15% error. Considering formal error propagation and the uncertainties in our peak-fitting algorithm, we estimate that the abundances given in Table 1 are accurate to about a factor of 2. The fit of a mass spectrum whose peaks result from the superposition of different molecular species is intrinsically degenerate, with several possible solutions (10).

Table 1. The 16 molecules used to fit the COSAC mass spectrum.

Name	Formula	Molar mass (u)	MS fraction	Relative to water
Water	H2O	18	80.92	100
Methane	CH4	16	0.70	0.5
Methanenitrile (hydrogen cyanide)	HCN	27	1.06	0.9
Carbon monoxide	CO	28	1.09	1.2
Methylamine	CH3NH2	31	1.19	0.6
Ethanenitrile (acetonitrile)	CH3CN	41	0.55	0.3
Isocyanic acid	HNCO	43	0.47	0.3
Ethanal (acetaldehyde)	CH3CHO	44	1.01	0.5
Methanamide (formamide)	HCONH2	45	3.73	1.8
Ethylamine	C2H5NH2	45	0.72	0.3
Isocyanomethane (methyl isocyanate)	CH3NCO	57	3.13	1.3
Propanone (acetone)	CH3COCH3	58	1.02	0.3
Propanal (propionaldehyde)	C2H5CHO	58	0.44	0.1
Ethanamide (acetamide)	CH3CONH2	59	2.20	0.7
2-Hydroxyethanal (glycolaldehyde)	CH2OHCHO	60	0.98	0.4
1,2-Ethanediol (ethylene glycol)	CH2(OH)CH2(OH)	62	0.79	0.2

The absence of large quantities of NH3, HCHO, and CO2 in our best fit may seem surprising because they were expected to be present as components of cometary ice. NH3 (m/z 17) was not needed for the fit, but the presence of small quantities seems likely. However, this is hard to quantify because the large H2Opeak atm/z 18 implies a substantial contribution to the m/z 17 peak from the OH fragment peak of H2O, which is difficult to distinguish from any NH3 contribution. HCHO (m/z 30) and CO2 (m/z 44) are not included because m/z 30 is mainly accounted for by fragment peaks of other molecules, rather than by the molecular ion of HCHO, and m/z 44 is mainly accounted for by fragment contributions from acetamide, formamide, and acetaldehyde, rather than by CO2.

We initially tried a fit that started with the assumption that m/z 44 came from CO2, but no acceptable fit could be achieved to the remaining peaks. If all of m/z 44 were ascribed to CO2, our sample would only contain 3% of CO2 relative to water. Using the procedure described above, we found that a more sensible fit for all mass peaks, especially m/z 57, 58, and 59, could only be achieved by assuming a CO2 concentration of less than 0.1%. The low abundance of CO2, NH3, and HCHO could indicate that the excavated COSAC sample came from an area depleted in volatile ice components. Observations by the Visible, Infrared and Thermal Imaging Spectrometer (VIRTIS) from the Rosetta orbiter (15) do suggest a dark surface depleted in volatiles, consisting mainly of refractory organic macromolecular materials, with very little ice on the surface. Studies (16) using the Rosetta Orbiter Spectrometer for Ion and Neutral Analysis (ROSINA) indicate that volatile ices sublime diurnally and seasonally, with CO2 ranging from 3% relative to water in local summer (the present case) to 80% in local winter.

The COSAC findings differ from those of Ptolemy (17) because COSAC sampled particles excavated by the impact (10) that entered the warm exhaust tubes located on the bottom of the lander, where they pointed toward the surface, whereas Ptolemy sampled ambient coma gases entering exhaust tubes located on top of the lander, where they pointed toward the sky (possibly with the addition of some dust that made its way around the lander). That COSAC detected far more nitrogen bearing compounds than Ptolemy agrees with

earlier observations that nitrogen was more abundant in the dust than in the gas of comet Halley (18). The Ptolemy team interpret their mass spectrum as fragments of polyoxymethylene polymer, with a strong CO2 peak of intensity 20% relative to water. COSAC did not detect ambient coma gases (which were dominated in Ptolemy data by CO2 with a few polymer fragments). The COSAC MS maintains a constant pressure; thus, subliming gases from our ground sample pushed the ambient coma gases outside the COSAC MS. Before sublimation, the total pressure inside the COSAC MS was dominated by CO2, in line with Ptolemy data and prelanding COSAC spectra. After sublimation, the total pressure inside the COSAC MS was due to the sum of the partial pressures of all the sublimed ground materials. This can explain the missing CO2 in the post-touchdown spectrum. The displacement of ambient coma gases by subliming ground materials and the temperature of 12° to 15°C in the COSAC exhaust tubes, which is too low to break down any refractory polymers in the ground materials, combine to explain why COSAC did not detect any polymer fragments.

The COSAC molecules form a consistent set related by plausible formation pathways (Fig. 3). A nitrogen source such as NH3 must originally have been abundant to form the many N-bearing species, but could since have mostly evaporated or been used up in reactions. All the COSAC organics can be formed by UV irradiation and/or radiolysis of ices due to the incidence of galactic and solar cosmic rays: alcohols and carbonyls derived from CO and H2Oices (19), and amines and nitriles from CH4 and NH3 ices (20). Hydrolysis of nitriles produces amides, which are linked to isocyanates by isomerization.

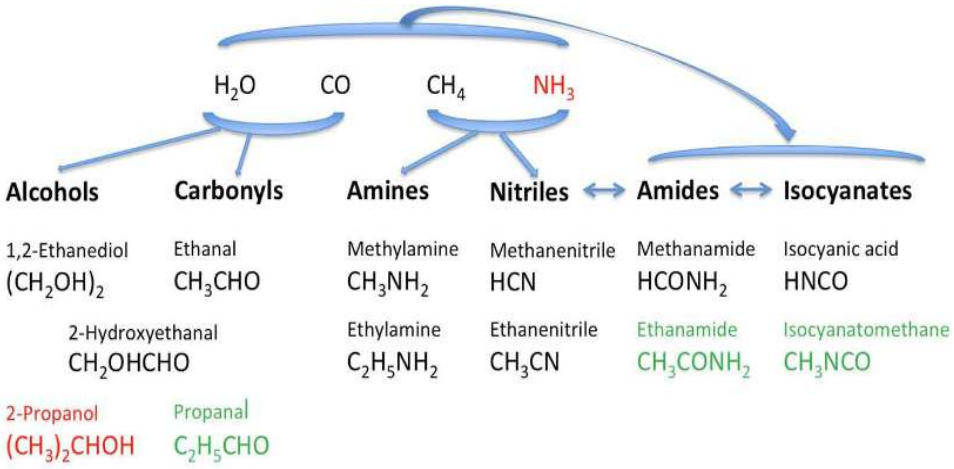

Figure 3. Possible formation pathways of COSAC compounds. Species in red are not confidently identified; species in green are reported for the first time in comets by COSAC.

Several of the COSAC compounds, such as HCN, CH3CN, and HNCO, are present in the comae of most comets (1). Others, such as CH3CHO, HCONH2, CH2(OH)CH2(OH), CH3NH2, and C2H5NH2, have only been found in a few comets. Four molecules reported by COSAC—CH3NCO, CH3COCH3, C2H5CHO, and CH3CONH2—have not been previously reported in a cometary environment, and CH2OHCHO has only been reported as an upper limit. These cometary molecules are all predicted by our generalized formation scheme (Fig. 3). CH2OHCHO is an efficient initiator in the prebiotic formation of sugars (21).

HCN is a key molecule in the prebiotic synthesis of amino acids (21, 22) and nucleobases (21) and even offers an elegant pathway to sugars (23). HCONH2 provides a prebiotic route to nucleobases (24). HCONH2 (24) and CH3CONH2 (21) catalyze phosphorylation of nucleosides to nucleotides, in which amines also play a role (21). Isocyanates play a major role in the prebiotic synthesis of peptides, through the so-called isocyanate route (22). The complexity of cometary nucleus chemistry and the importance of N-containing organics imply that early solar system chemistry fosters the formation of prebiotic material in noticeable concentrations.

REFERENCES AND NOTES

1. M. J. Mumma, S. B. Charnley, The chemical composition of comets—emerging taxonomies and natal heritage. Annu. Rev. Astron. Astrophys. 49, 471–524 (2011). doi: 10.1146/annurev-astro-081309-130811
2. J. Greenberg, Astron. Astrophys. 330, 375–380 (1998).
3. J. Crovisier et al., The chemical diversity of comets: Synergies between space exploration and ground-based radio observations. Earth Moon Planets 105, 267–272 (2009). doi: 10.1007/s11038-009-9293-z
4. M. DiSanti, M. Mumma, Reservoirs for comets: Compositional differences based on infrared observations. Space Sciences Series 28, 127–145 (2008). doi: 10.1007/978-0-387-85455-7_8
5. J. Oró, T. Mills, A. Lazcano, Comets and the formation of biochemical compounds on the primitive Earth—a review. Orig. Life Evol. Biosph. 21, 267–277 (1992). doi: 10.1007/ BF01808302; pmid: 11537542
6. W. M. Irvine, Extraterrestrial organic matter: A review. Orig. Life Evol. Biosph. 28, 365–383 (1998). doi: 10.1023/A:1006574110907; pmid: 9742722
7. F. Goesmann et al., Cosac, The cometary sampling and composition experiment on Philae. Space Sci. Rev. 128, 257–280 (2007). doi: 10.1007/s11214-006-9000-6
8. F. Goesmann et al., Interpretation of COSAC mass spectrometer data acquired during Rosetta's Lutetia fly-by 10 July 2010. Planet. Space Sci. 66, 187–191 (2012). doi: 10.1016/j.pss.2012.01.012
9. J. Biele et al., The landing(s) of Philae and inferences on comet surface mechanical properties. Science 349, 10.1126/science.aaa9816 (2015).
10. Full details and methods are in the supplementary materials.
11. S. E. Stein, in NIST Chemistry WebBook, NIST Standard Reference Database Number 69, P. J. Linstrom, W. G. Mallard, Eds. (National Institute of Standards and Technology, Gaithersburg, MD); http://webbook.nist.gov.
12. J. H. Waite Jr. et al., Ion neutral mass spectrometer results from the first flyby of Titan. Science 308, 982–986 (2005). doi: 10.1126/science.1110652; pmid: 15890873
13. K. E. Mandt et al., Ion densities and composition of Titan's upper atmosphere derived from the Cassini Ion Neutral Mass Spectrometer: Analysis methods and comparison of measured ion densities to photochemical model simulations. J. Geophys. Res. Solid Earth 117 (E10), E10006 (2012). doi: 10.1029/2012JE004139
14. J. H. Waite Jr. et al., Cassini ion and neutral mass spectrometer: Enceladus plume composition and structure. Science 311, 1419–1422 (2006). doi: 10.1126/science.1121290; pmid: 16527970
15. F. Capaccioni et al., The organic-rich surface of comet 67P/Churyumov-Gerasimenko as seen by VIRTIS/Rosetta. Science 347, (2015) 10.1126/science.aaa0628. pmid: 25613895
16. M. Hässig et al., Time variability and heterogeneity in the coma of 67P/Churyumov-Gerasimenko. Science 347, aaa0276 (2015). doi: 10.1126/science.aaa0276; pmid: 25613892
17. I. P. Wright et al., CHO-bearing organic compounds at the surface of 67PChuryumov-Gerasimenko revealed by Ptolemy. Science 349, 10.1126/science.aab0673 (2015).
18. S. Wyckoff, S. C. Tegler, L. Engel, Nitrogen abundance in Comet Halley. Astrophys. J. 367, 641–648 (1991). doi: 10.1086/169659
19. G. M. Muñoz Caro, E. Dartois, Prebiotic chemistry in icy grain mantles in space. An experimental and observational approach. Chem. Soc. Rev. 42, 2173–2185 (2013). doi: 10.1039/c2cs35425j; pmid: 23340705
20. Y. S. Kim, R. I. Kaiser, On the formation of amines (RNH2) and the cyanide anion (CN–) in electron-irradiated ammonia-hydrocarbon interstellar model ices. Astrophys. J. 729, 68–75 (2011). doi: 10.1088/0004-637X/729/1/68
21. L. E. Orgel, Prebiotic chemistry and the origin of the RNA world. Crit. Rev. Biochem. Mol. Biol. 39, 99–123 (2004). doi: 10.1080/10409230490460765; pmid: 15217990
22. R. Pascal, L. Boiteau, A. Commeyras, From the prebiotic synthesis of *a*-amino acids towards a primitive translation apparatus for the synthesis of peptides. Top. Curr. Chem. 259, 69–122 (2005). doi: 10.1007/b136707
23. D. Ritson, J. D. Sutherland, Prebiotic synthesis of simple sugars by photoredox systems chemistry. Nat. Chem. 4, 895–899 (2012). doi: 10.1038/nchem.1467; pmid: 23089863

24. R. Saladino, C. Crestini, F. Ciciriello, G. Costanzo, E. Di Mauro, Formamide chemistry and the origin of informational polymers. Chem. Biodivers. 4, 694–720 (2007). doi: 10.1002/cbdv.200790059; pmid: 17443884

ACKNOWLEDGMENTS

This work was supported by Deutsches Zentrum für Luft- und Raumfahrt (DLR) under contract no. 50 QP 1302, and by Centre National d'Etudes Spatiales (CNES) grants at LATMOS and LISA. U.J. M. was funded by L'Agence Nationale de la Recherche (ANR-12-IS07-0006). Support from the NASA Astrobiology Institute (P.E.), the NASA Postdoctoral Program at Goddard Space Flight Center (T.G.), Programme de Développement d'Expériences scientifiques through Enterprise Ireland (S.McK.L.), and the Welch Foundation (A.J.MacD.) is acknowledged. Rosetta is a European Space Agency (ESA) mission with contributions from member states and NASA. The Philae lander was provided by a consortium led by DLR, Max-Planck-Institut für Sonnensystemforschung, CNES, and Agenzia Spatiale Italiana. The data used in this study are available through ESA's Planetary Science Archive (www.rssd.esa.int/index.php?project=PSA&page=rosetta).

SUPPLEMENTARY MATERIALS

See below and https://hal.science/insu-01182551
Materials and Methods
Figs. S1 and S2
Tables S1 to S4
References (25–32)

Supplementary Materials for

Organic compounds on comet 67P/Churyumov-Gerasimenko revealed by COSAC mass spectrometry

Fred Goesmann,* Helmut Rosenbauer, Jan Hendrik Bredehöft, Michel Cabane, Pascale Ehrenfreund, Thomas Gautier, Chaitanya Giri, Harald Krüger, Léna Le Roy, Alexandra J. MacDermott, Susan McKenna-Lawlor, Uwe J. Meierhenrich, Guillermo M. Muñoz Caro, Francois Raulin, Reinhard Roll, Andrew Steele, Harald Steininger, Robert Sternberg, Cyril Szopa, Wolfram Thiemann, Stephan Ulamec

*Corresponding author. E-mail: goesmann@mps.mpg.de

Published 31 July 2015, *Science* **349**, aab0689 (2015)
DOI: 10.1126/science.aab0689

This PDF file includes:

Tables S1 to S3 (Excel)

Materials and Methods

Measurement Strategy

The sequence of instrument activities was fixed before landing. The COSAC sniffing was intended to be the first measurement after nominal landing costing little energy and time. In addition no knowledge about the Lander situation was required. This sequence was triggered automatically by the generation of the touch down signal from Philae. The MS sniffing procedure did not involve any active sampling or heating, but was simply a switch on of the mass spectrometer in order to sample the gas environment present in the instrument's ion source.

After an initial characterization of the landing site and preliminary data evaluation on Earth, drilling would be attempted and a proper soil sample delivery to COSAC was scheduled. All these procedures and time lines were fixed well in advance to landing. This sequence would have delivered a full GC-MS data set. Due to the non-nominal landing this did not happen. The sniffing measurement reported here is the most organic containing data set COSAC retrieved on the comet up to now.

Suggested Sample Delivery

At the first touch-down of Philae a significant amount of material was excavated (about 0,4 m³, (*10*)). Grains almost certainly entered the exhaust pipes of COSAC, which have orifices with an inner diameter of 19 mm at the baseplate (i.e. "bottom side") of the Lander. These grains would have stuck to the inside of the tubes, most likely at a position where the temperature was at ~ 12-15°C. (This temperature can be derived from the Philae thermal model and measurements made nearby the tubes, i.e. at the mass spectrometer, the baseplate and the instrument panels to which COSAC is attached. Note that the low thermal conductivity of the plastic tubes (0.000092 W/K) helps to insulate the warm interior from the cold exterior of the Lander, which was at the time of landing about -90°C, thereby leading to an intermediate temperature in the bent part of the pipe close to that of the MS. Trapped gases would thereafter have evolved which could be measured in the MS, some 25 min later. This explains differences between the COSAC measurements and those performed by Ptolemy at about the same time, where the sniffing was performed through a pipe to the top of the Lander (*17*).

Calculation of Peak Intensities of COSAC FSS Mass Spectrum of 12 Nov 2014

In the initial step the spectrum was mass calibrated through a mathematical treatment that transforms the intensity versus time data into a mass spectrum with intensity plotted versus mass per unit charge. We calculate peak intensities in an automated way. First a mass calibration of the spectrum is obtained with peaks at m/z 1, 18, 28, 44, assuming that these peaks are due to hydrogen, water, carbon monoxide and carbon dioxide. In order to obtain the masses of these peaks we fit Gaussians to each and calculate the peak center from the full-width at half-maximum of each fitted Gaussian profile. In order to check the influence of our peak identification at m/z 44, we applied an alternative mass calibration assuming that the peak at m/z 44 is entirely due to C_3H_8, the heaviest possible ion at this mass, leaving the other calibration peaks unchanged. The resulting shift in the

mass calibration is negligible and affects neither our peak identification nor the deduced peak intensities. This data set is then treated further using this particular mass scale. To obtain the total intensity in a selected peak, a mass window is defined that is centered close to the integer *m*/*z* of that peak. For noise background determination close to the peak, we define two windows that are offset from the main peak window towards lower and higher *m*/*z* values, respectively.

We set the window size so that the number of spectrum channels is independent of *m*/*z* up to *m*/*z* 60 and take 40 spectrum channels in the peak window and 15 channels in each of the background windows. Due to the decreasing mass resolution of the time-of-flight spectrum towards higher masses we have to increase the widths of the windows on the *m*/*z* scale in order to keep the number of spectrum channels constant. This guarantees that the statistical uncertainty in each window type (peak or background) is independent of *m*/*z*.

With increasing mass the background windows move closer to the background windows of adjacent peaks, and, beginning at $m/z > 40$, these background windows partially overlap. At *m*/*z* 60 the background windows from adjacent peaks completely overlap and entirely fill the gap between the peak windows. Therefore, for $m/z > 60$ the widths of the peak and the background windows have to be reduced. We calculate the total intensity in the peak and in each of the background windows as the sum of the counts in the spectrum channels covered by each of the three windows. We take the background intensity at the peak location as the average of the two background values and subtract the resulting number from the peak intensity. We calculate this background-subtracted peak intensity for each *m*/*z* in integer steps.

The resulting peak list, see Table S1, gives the background-subtracted peak intensity up to *m*/*z* 120. Entries below about 20 counts are in the range of the statistical limit of this method, as one may see from the occurrence of negative entries in the peak list down to −20 counts. For example, for *m*/*z* 102, the plotted spectrum shows a very weak peak, while the peak list gives only 2 counts for this mass. Since the COSAC MS consistently produced constant instrument background signals at *m*/*z* 18, 28, and 44 (*8*), even during hibernation, these values need to be subtracted, as was done in Table S1.

Mass Fragmentation Pattern and Reduction Strategy

The identification of molecules from a single mass spectrum containing several compounds is intrinsically degenerate. In order to arrive at a plausible composition we used exclusion principles. Some are rather strict and convincing, some less so.
The mass fragmentation patterns of the molecules were retrieved from the National Institute of Standards and Technology (NIST) database (*11*), and used for COSAC analysis as described in (25). Molecules giving strong signals where the COSAC mass spectrum shows only noise were discarded, as were molecules showing strong signals where the COSAC signals were weak. Compounds showing peaks in the mass range above *m*/*z* 62 were omitted. Compounds containing chlorine, fluorine and boron were omitted, as their signals were indistinguishable from instrument noise.

The color coding scheme used in tables S1 – S3 distinguishes between different reasons to adopt particular molecular choices.
Table S1: file: COSAC_Table_S_1.xlsx
In this table the original intensity values are displayed and a large series of molecules and their fragmentation patterns are listed. It contains a list of all the molecules we considered to be possible candidates within the mass range observed. This list was reduced following the reasons listed in table S3, leaving us with table S2
Table S2: file: COSAC_Table_S_2.xlsx
This table contains the reduced list. Three compounds were added in order to list the fragmentation patterns of Glycine, Alanine, and 2-oxo-butanoic acid.
Table S3: file: COSAC_Table_S_3.xlsx
This table contains an explicit reason for deleting each of the molecules removed from table S1 in order to form table S2.

The Fit

In order to explain the way the spectrum was fitted, the considerations leading to the molecular choices made from the tables are listed in very short form below starting from mass 59 downwards. This explanation ends at *m*/*z* 27 but the general idea should be clear. Our protocol to identify molecular species, based on the data collected by the COSAC mass spectrometer after the first touchdown, made use of the NIST MS database. Molecules with no available mass spectrum in this database were not included in our fit, the HNCO compound being the only exception. It was found that, in general, our mass spectra of various standard species were comparable to those provided by the NIST (25). The fit of the mass spectrum, which is composed of a set of peaks which contain contributions from different molecular species, has no unique solution. It is therefore not possible to provide a definitive list of molecules that fits our data. The following criteria were thus applied to reduce the number of potential molecular candidates to species that were detected with a high probability:

i) In general, we applied Occam´s razor, reducing as much as possible the number of species required to fit the mass spectrum.
ii) The fit was made in order of decreasing mass, starting from *m*/*z* 59. This way, the contributions of the fragments from the heavier molecules, e.g. acetamide (with a molecular ion mass of 59), to lower masses (the *m*/*z* 44, 43 signals are also in the spectrum of acetamide) are accounted for. Then, if the signal intensity of these lower *m*/*z* values needed an additional contribution, a new molecule was introduced. Many potential candidates for a given *m*/*z* value were discarded because their contribution to other *m*/*z* values was excessive and, therefore, did not fit the spectrum.
iii) The most unstable species and the organic molecules with unsaturated carbon-carbon bonds were avoided. It would be unlikely to detect the unsaturated molecule and not its saturated version.

All *m*/*z* peaks in the mass spectrum could be well fitted using sixteen species, except *m*/*z* 15 and a fraction of *m*/*z* 57, see Fig. 2. The percentages given in Table 1 are the molecular abundances relative to that of water in the sample. These values were corrected for electron ionization cross sections. The molecular assignment of the mass

fragments detected in the spectrum after the first touchdown followed the above criteria. A short discussion of this assignment is given below. It is important to note that for brevity, a large number of the molecules taken into consideration are not mentioned here. However, all the molecules with a reported spectrum were taken into consideration for the fit before ruling them out. For a specific molecule, the intensity of a fragment, *m/z*, in the mass spectrum is relative to the main peak intensity value (100%), indicated in parentheses:

m/z 60
Small peak close to the noise level, no species from the NIST database with molecular *m/z* 60 is an important contributor to *m/z* 59, 58, 57. The absence of a significant signal for *m/z* 60 indicates that acetic acid (CH_3COOH) and methyl formate ($HCOOCH_3$) abundances, with respective *m/z* 60 intensities of 75% and 38%, are negligible. Glycol aldehyde ($HOCH_2CHO$), with *m/z* 60, has a small intensity of *m/z* 60; it was considered in the fit, see comment on *m/z* 31.

m/z 59
The best candidate is acetamide ($CH_3(C=O)NH_2$, *m/z* 59) for this fragment. It contributes mainly to *m/z* 59 (100%), 44 (99%), 43 (60%), and 42 (31%). Acetamide therefore contributes to the 2 series of 3 peaks each in the mass spectrum, in particular to *m/z* 59 (molecular ion), 44 (CH_2NO+), and 43 (C_2H_3O+).

N-methylformamide ($HCONHCH_3$) could account for at most 50% of *m/z* 59, based on the ratio *m/z* 59/30 = 100/54 for this molecule, which is close to 1/1 in our spectrum. It was not included in the fit because methylamine already fits *m/z* 30 and, in addition, 31. Similarly, propylamine ($CH_3CH_2CH_2NH_2$), has a small *m/z* 59 peak (9%) compared to *m/z* 30 (100%), it would contribute by no more than 10% to the *m/z* 59 fit. N,N-dimethyl-methylamine or trimethylamine could add to *m/z* 59 (68%) and 58 (100%), but contributes in excess to *m/z* 42 (25%) and was therefore not used for the fit.

m/z 58
Potential contributors to this fragment are trimethylamine (100%), glyoxal (44%), methoxyethene (77%), and propanal (100%). Trimethylamine, $(CH_3)_3N$, was discarded because *m/z* 42 is about 25% and this peak is not clearly present in our data. Glyoxal (O=CH-CH=O) could contribute to *m/z* 58, 44, and 43 while its main intensities fall at *m/z* 29, 31, and 30, but added in excess, in particular to *m/z* 32 (25%) which is not clearly present in our data. Methoxyethene ($CH_3OCH_2CH_3$) with main peaks at *m/z* 58, 43, and 15 could partially contribute. The species 2-propanamine with *m/z* 58 (8%), adds in excess to *m/z* 44 (100%), and 42 (17%) and was neglected. The HCOOCH radical anion of $HCOOCH_3$ was discarded, see above. Propenol (C_3H_6O) could contribute mainly to 57, little to 58, but it is an unsaturated species and there is no clear evidence for the presence of propanol. Propanal (CH_3CH_2CHO) has its main fragment at *m/z* 58 and has a significant signal at *m/z* 57 (30%), 29 (88%), 28 (58%), and 27 (47%), it was included in our fit. Acetone ($CH_3(C=O)CH_3$) with *m/z* 43 as main fragment was also selected for the fit, it adds appreciably to *m/z* 58 (25%).

Regarding simple aliphatic chain species with no functional groups, butane (C_4H_{10}) with *m*/*z* 58 contributes mainly to *m*/*z* 43 and may be present. Propane (C_3H_8) has a strong signal at *m*/*z* 29, which is intense in our spectrum, while ethane (C_2H_6) would contribute mainly to *m*/*z* 28. Pentane's contribution is negligible because its spectrum has *m*/*z* 41 and 42 near 60% and these signals are weak in our data.

m/*z* 57

Only the mass spectra of propenol (C_3H_6O) or methyl isocyanate and its isomers (C_2H_3NO) display *m*/*z* 57 as the main fragment. Propenol has [57, 100%] and [58, 23%], while methyl isocyanate (O=C=N-CH_3) has [56, 37%] and [57, 100%]. The intensity of peak *m*/*z* 57 is not accounted for while fitting *m*/*z* 59 and 58. We are thus forced to include at least one of those two candidates, but propenol was discarded, see above comment for fragment *m*/*z* 58. Methyl isocyanate was therefore included. As outlined below HNCO (H-N=C=O, isocyanic acid) is a plausible candidate and methyl isocyanate ((O=C=N-CH_3)) might be formed by methylation of HNCO. However, methyl isocyanate cannot be the only contributor to *m*/*z* 57 because of its 56/57 ratio compared to our spectrum with a weak *m*/*z* 56 intensity. Other potential candidates that were not included are: hydroxy-acetonitrile ($HOCH_2CN$) with *m*/*z* 28 (100%) and 56 (22%), because *m*/*z* 56 is weak in our data; and 2-propen-1-amine and cyclopropylamine, because their main mass fragment is *m*/*z* 56.

m/*z* 45

Formamide ($HCONH_2$) was found to be the best candidate. In addition, the above identification of acetamide suggests there could be also formamide, which would contribute mainly to *m*/*z* 45, 44 and 29. Nitrosomethane (CH_3-N=O) has *m*/*z* 45 of about 70% relative to *m*/*z* 30 It could contribute to *m*/*z* 45 but not sufficiently because *m*/*z* 30 is weaker than *m*/*z* 45 in our data. Dimethylamine (CH_3-NH-CH_3) has *m*/*z* 45 of 63% relative to *m*/*z* 44. It could also be present but contributes to an excess in the fit of *m*/*z* 44 and 42. Therefore formamide is the preferred choice. Ethylamine was also included in the fit, but it contributes mainly to *m*/*z* 30 and has in comparison a low intensity for *m*/*z* 45 (19%).

m/*z* 44

CO_2 is the obvious candidate, but molecules used to fit higher masses, in particular acetamide and formamide, accounted for much of the *m*/*z* 44 peak in our spectrum. There is a very reduced number of organic molecules with *m*/*z* 44 as the molecular mass. Only acetaldehyde (CH_3CHO) with *m*/*z* 44 was found to add significantly to *m*/*z* 44; its main fragments are *m*/*z* 44 (82%), 43 (47%), and 29 (100%).

m/*z* 43

Some selected species with higher masses (acetamide, formamide, acetaldehyde, and acetone) contribute significantly to 43. No real candidate with a molecular mass of *m*/*z* 43 was found in the NIST database. Acetone ($CH_3(C=O)CH_3$) has a mass of *m*/*z* 58, but its main fragment is *m*/*z* 43, while other fragments in its spectrum are negligible. It contributes only partially to *m*/*z* 43 because it would otherwise add in excess to *m*/*z* 42 (already fitted with acetamide) and *m*/*z* 58 (fitted with methylamine). Thus it was

selected along with HNCO to fit *m/z* 43. HNCO is a good candidate because it has its main peak at *m/z* 43 being *m/z* 29 about 30%), other peaks in the HNCO spectrum are below 20% in intensity relative to *m/z* 43 *(26)*

m/z 41
Acetonitrile (CH_3CN) has a molecular mass of *m/z* 41, *m/z* 41 being its main fragment, while *m/z* 40 is near 50%. There is only a minor contribution from other mass fragments in its spectrum. It was therefore included in the fit. Its methyl isocyanide isomer (CH_3NC) might also contribute. No other candidate molecules with *m/z* 41 were found.

m/z 32
The absence of a clear signal around *m/z* 32 indicates that Sulfur-bearing species were not detected in our measurement.

m/z 31
Methylamine has a mass of *m/z* 31, *m/z* 30 being its main fragment, it also contributes significantly to *m/z* 31 (65%) and 28 (54%). It was the only candidate found with a molecular mass of *m/z* 31 and is required to account for the intensity of *m/z* 31. Glycol aldehyde ($HOCH_2CHO$) was also included in the fit because its main fragment is *m/z* 31, its abundance is limited because it also contributes to *m/z* 32 (48%) and 60 (7%) and both masses have a very low intensity in the measured spectrum. The same holds for ethylene glycol ($HOCH_2CH_2OH$), where in this case its contribution to *m/z* 31 is limited by its spectral intensity for *m/z* 33 (36%). Glyoxal (O=CH-CH=O), with *m/z* 31 (86%) and main peak at *m/z* 29, was not considered because it would lead to excess in the fit of other fragments, see comment for *m/z* 58.

m/z 29
Propanal (C_2H_5CHO), used to fit *m/z* 58, is the main contributor to the *m/z* 29 fragment.

m/z 28
Carbon monoxide was expected to contribute, since it was detected in previous cometary measurements. In addition, other species with larger masses required to fit the spectrum contribute to this fragment.

m/z 27
After entering all the molecular candidates with higher masses, the intensity of *m/z* 27 (and *m/z* 15) was under-fitted. Hydrogen cyanide (HCN) is the only good candidate with this mass, its main peak is at *m/z* 27 and other fragments have minor intensities.

Mathematical Procedure for semi-quantitative Analysis
In order to convert mass fragment intensities to molar abundances, the probabilities of forming and thereafter detecting a fragment need to be taken into account. The ionization of a compound in the ionizing chamber of the instrument depends on a number of parameters, one of which is compound-specific. Electron current density and electrode geometry are identical for all compounds, so they do not need to be considered in a comparison between several different compounds in the same spectrum. The compound-

specific parameter utilized is its electron-impact cross section σ at 70 eV (as employed in the instrument). A second parameter determining intensity in a mass spectrum is mass discrimination, which involves a different permeability or detector gain for different masses. Time-of-flight instruments such as COSAC, typically show no, or only minimal, mass discrimination, so for the rather small mass window concerned here we assume an identical detection probability for all masses. Thus, the only correction necessary is the division of mass spectrum intensities by the electron impact cross section σ for each compound. Since there are no experimental data available for a number of relevant compounds, all values of σ used in this analysis were calculated using quantum chemical models. The model used is the Binary-Encounter-Bethe (BEB) model, as described in *(27)* and *(28)*. In a deviation from this model, all molecular orbitals were included in the present calculation. The process used consisted of three steps. First, the geometry of the molecule was optimized using a Restricted Hartree Fock (RHF) calculation with a 6-311++G(sd,p) basis set. To confirm that the energy minimum identified was indeed the global minimum, in a second step a B3LYP Density Functional Theory (DFT) calculation of both, the ground state and the first cationic state with the same geometry, was performed. The energy difference between the two states then comprises the vertical excitation potential, which should be slightly higher than the first ionization potential (IP). The calculated energy difference was compared with experimental data from the NIST webbook database *(29)*. When the energy difference was small (<0.2 eV), a third and final step was made consisting of an RHF single point energy calculation and virial analysis of the molecule, which procedure yielded all the parameters then required to calculate σ_{BEB}. When possible, the calculated values were compared with experimental data and these comparisons showed good agreement. All calculations were performed using the GAMESS software package *(30)* and *(31)*.

Fig. S1.

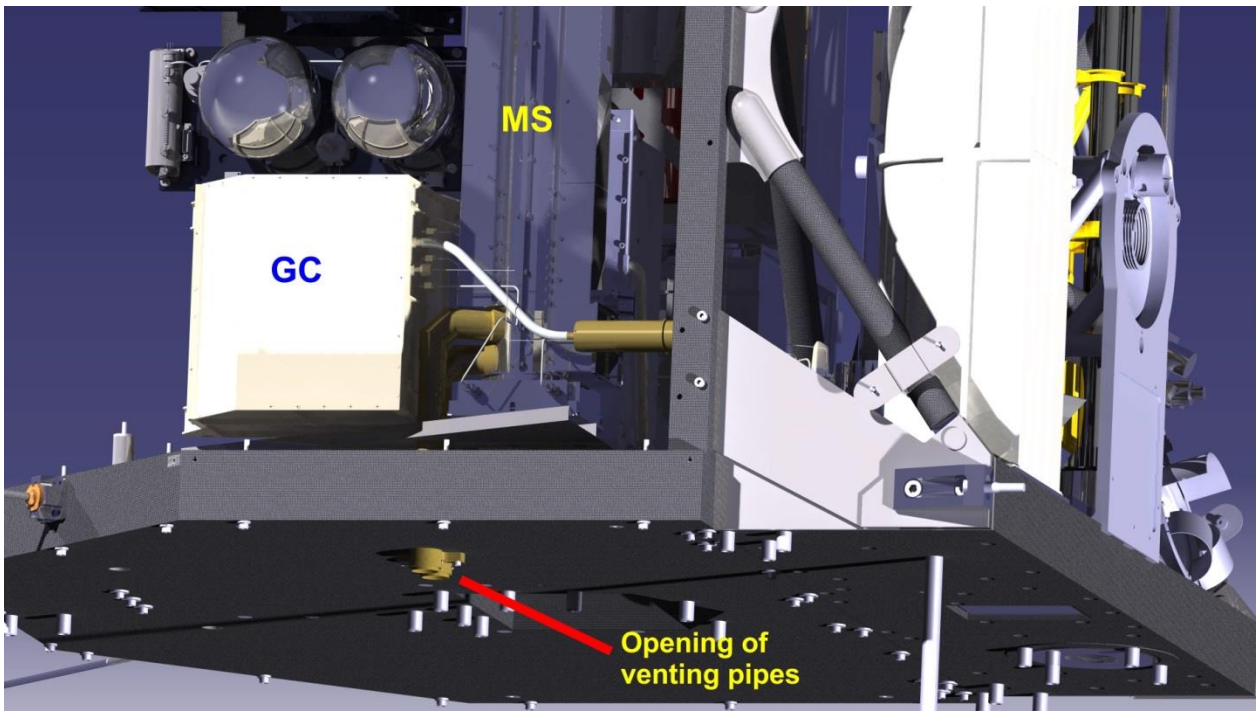

Figure S1: Lander body including COSAC elements and the venting pipes. The openings of the pipes are at the baseplate, pointing "downwards" so that ejected material from the surface could easily enter. The grains would then stick somewhere on the inside surfaces of the pipes, where temperatures were around 12-15°C.

Fig. S2

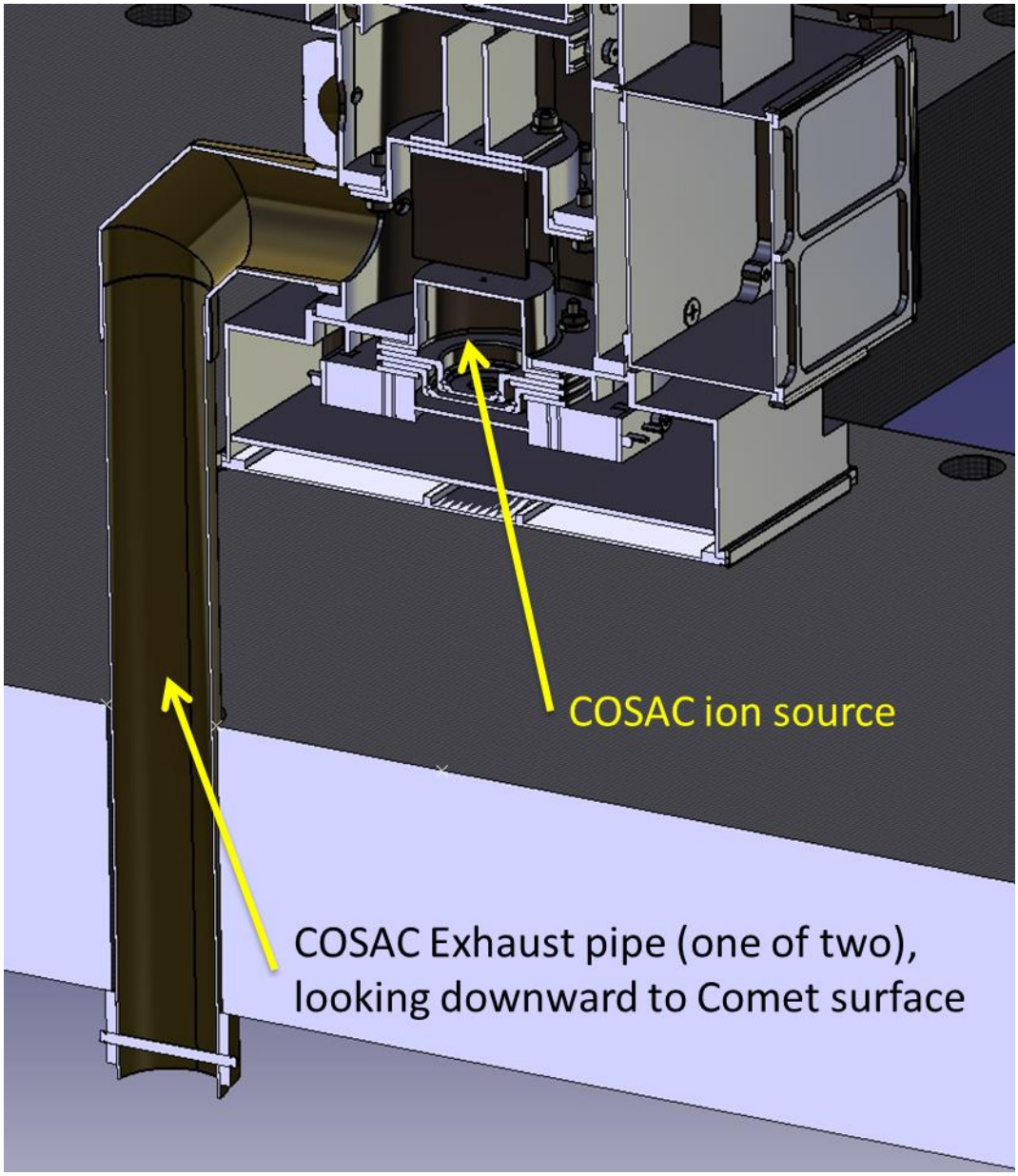

Figure S2: Cross section of the COSAC exhaust; the image shows one of the exhaust tubes in cross section (19 mm inner diameter) where cometary dust could have entered. It also shows the geometry of the ion source of the mass spectrometer.

Table S4.

The following cross sections were used in the analysis:

Table S4: Electron-impact cross sections σ_{BEB} as used in this study.

Compound	σ_{BEB} [Å²]	***Measured ****	***Deviation***
Acetaldehyde	6.94	6.93	0.14%
Acetamide	9.72		
Acetone	9.94	10.20	-2.55%
Acetonitrile	6.16		
Ammonia	3.55		
Carbon monoxide	2.84	2.99	-5.02%
Carbon dioxide	3.97	4.05	-1.98%
Ethylamine	9.07		
Ethylene glycol	10.42		
Formaldehyde	4.13		
Formamide	6.60		
Glycolaldehyde	8.52		
Hydrogen cyanide	3.53		
Isocyanic acid	4.87		
Isocyanatomethane	7.55		
Methane	4.40	4.67	-5.78%
Methanol	5.42		
Methylamine	6.77		
Propanal	9.82	9.38	4.69%
Water	2.53		

* Measured values are from the literature *(32)*

References and Notes

1. M. J. Mumma, S. B. Charnley, The chemical composition of comets—emerging taxonomies and natal heritage. *Annu. Rev. Astron. Astrophys.* **49**, 471–524 (2011). doi:10.1146/annurev-astro-081309-130811

2. J. Greenberg, *Astron. Astrophys.* **330**, 375–380 (1998).

3. J. Crovisier, N. Biver, D. Bockelée-Morvan, J. Boissier, P. Colom, D. C. Lis, The chemical diversity of comets: Synergies between space exploration and ground-based radio observations. *Earth Moon Planets* **105**, 267–272 (2009). doi:10.1007/s11038-009-9293-z

4. M. DiSanti, M. Mumma, Reservoirs for comets: Compositional differences based on infrared observations. *Space Sciences Series* **28**, 127–145 (2008). doi:10.1007/978-0-387-85455-7_8

5. J. Oró, T. Mills, A. Lazcano, Comets and the formation of biochemical compounds on the primitive Earth—a review. *Orig. Life Evol. Biosph.* **21**, 267–277 (1992). Medline doi:10.1007/BF01808302

6. W. M. Irvine, Extraterrestrial organic matter: A review. *Orig. Life Evol. Biosph.* **28**, 365–383 (1998). Medline doi:10.1023/A:1006574110907

7. F. Goesmann, H. Rosenbauer, R. Roll, C. Szopa, F. Raulin, R. Sternberg, G. Israel, U. Meierhenrich, W. Thiemann, G. Munoz-Caro, Cosac, The cometary sampling and composition experiment on Philae. *Space Sci. Rev.* **128**, 257–280 (2007). doi:10.1007/s11214-006-9000-6

8. F. Goesmann, S. McKenna-Lawlor, R. Roll, J. H. Bredehöft, U. Meierhenrich, F. Raulin, W. Thiemann, G. M. Muñoz Caro, C. Szopa, Interpretation of COSAC mass spectrometer data acquired during Rosetta's Lutetia fly-by 10 July 2010. *Planet. Space Sci.* **66**, 187–191 (2012). doi:10.1016/j.pss.2012.01.012

9. J. Biele, S. Ulamec, M. Maibaum, R. Roll, L. Witte, E. Jurado, P. Muñoz, W. Arnold, H.-U. Auster, C. Casas, C. Faber, C. Fantinati, F. Finke, H.-H. Fischer, K. Geurts, C. Güttler, P. Heinisch, A. Herique, S. Hviid, G. Kargl, M. Knapmeyer, J. Knollenberg, W. Kofman, N. Kömle, E. Kührt, V. Lommatsch, S. Mottola, R. Pardo de Santayana, E. Remetean, F. Scholten, K. J. Seidensticker, H. Sierks, T. Spohn, The landing(s) of Philae and inferences on comet surface mechanical properties. *Science* **349**, aaa9816 (2015).

10. Full details and methods are in the supplementary materials on *Science* Online.

11. S. E. Stein, in *NIST Chemistry WebBook*, NIST Standard Reference Database Number 69, P. J. Linstrom, W. G. Mallard, Eds. (National Institute of Standards and Technology, Gaithersburg, MD); http://webbook.nist.gov.

12. J. H. Waite Jr., H. Niemann, R. V. Yelle, W. T. Kasprzak, T. E. Cravens, J. G. Luhmann, R. L. McNutt, W. H. Ip, D. Gell, V. De La Haye, I. Müller-Wordag, B. Magee, N. Borggren, S. Ledvina, G. Fletcher, E. Walter, R. Miller, S. Scherer, R. Thorpe, J. Xu, B. Block, K. Arnett, Ion neutral mass spectrometer results from the first flyby of Titan. *Science* **308**, 982–986 (2005). Medline doi:10.1126/science.1110652

13. K. E. Mandt, D. A. Gell, M. Perry, J. Hunter Waite Jr., F. A. Crary, D. Young, B. A. Magee, J. H. Westlake, T. Cravens, W. Kasprzak, G. Miller, J.-E. Wahlund, K. Ågren, N. J. T.

Edberg, A. N. Heays, B. R. Lewis, S. T. Gibson, V. de la Haye, M.-C. Liang, Ion densities and composition of Titan's upper atmosphere derived from the Cassini Ion Neutral Mass Spectrometer: Analysis methods and comparison of measured ion densities to photochemical model simulations. *J. Geophys. Res. Solid Earth* **117** (E10), E10006 (2012). doi:10.1029/2012JE004139

14. J. H. Waite Jr., M. R. Combi, W. H. Ip, T. E. Cravens, R. L. McNutt Jr., W. Kasprzak, R. Yelle, J. Luhmann, H. Niemann, D. Gell, B. Magee, G. Fletcher, J. Lunine, W. L. Tseng, Cassini ion and neutral mass spectrometer: Enceladus plume composition and structure. *Science* **311**, 1419–1422 (2006). Medline doi:10.1126/science.1121290

15. F. Capaccioni, A. Coradini, G. Filacchione, S. Erard, G. Arnold, P. Drossart, M. C. De Sanctis, D. Bockelee-Morvan, M. T. Capria, F. Tosi, C. Leyrat, B. Schmitt, E. Quirico, P. Cerroni, V. Mennella, A. Raponi, M. Ciarniello, T. McCord, L. Moroz, E. Palomba, E. Ammannito, M. A. Barucci, G. Bellucci, J. Benkhoff, J. P. Bibring, A. Blanco, M. Blecka, R. Carlson, U. Carsenty, L. Colangeli, M. Combes, M. Combi, J. Crovisier, T. Encrenaz, C. Federico, U. Fink, S. Fonti, W. H. Ip, P. Irwin, R. Jaumann, E. Kuehrt, Y. Langevin, G. Magni, S. Mottola, V. Orofino, P. Palumbo, G. Piccioni, U. Schade, F. Taylor, D. Tiphene, G. P. Tozzi, P. Beck, N. Biver, L. Bonal, J. P. Combe, D. Despan, E. Flamini, S. Fornasier, A. Frigeri, D. Grassi, M. Gudipati, A. Longobardo, K. Markus, F. Merlin, R. Orosei, G. Rinaldi, K. Stephan, M. Cartacci, A. Cicchetti, S. Giuppi, Y. Hello, F. Henry, S. Jacquinod, R. Noschese, G. Peter, R. Politi, J. M. Reess, A. Semery, Cometary science. The organic-rich surface of comet 67P/Churyumov-Gerasimenko as seen by VIRTIS/Rosetta. *Science* **347**, aaa0628 (2015). Medline

16. M. Hässig, K. Altwegg, H. Balsiger, A. Bar-Nun, J. J. Berthelier, A. Bieler, P. Bochsler, C. Briois, U. Calmonte, M. Combi, J. De Keyser, P. Eberhardt, B. Fiethe, S. A. Fuselier, M. Galand, S. Gasc, T. I. Gombosi, K. C. Hansen, A. Jäckel, H. U. Keller, E. Kopp, A. Korth, E. Kührt, L. Le Roy, U. Mall, B. Marty, O. Mousis, E. Neefs, T. Owen, H. Rème, M. Rubin, T. Sémon, C. Tornow, C. Y. Tzou, J. H. Waite, P. Wurz, Time variability and heterogeneity in the coma of 67P/Churyumov-Gerasimenko. *Science* **347**, aaa0276 (2015). Medline doi:10.1126/science.aaa0276

17. I. P. Wright, S. Sheridan, S. J. Barber, G. H. Morgan, D. J. Andrews, A. D. Morse, CHO-bearing organic compounds at the surface of 67PChuryumov-Gerasimenko revealed by Ptolemy. *Science* **349**, aab0673 (2015).

18. S. Wyckoff, S. C. Tegler, L. Engel, Nitrogen abundance in Comet Halley. *Astrophys. J.* **367**, 641–648 (1991). doi:10.1086/169659

19. G. M. Muñoz Caro, E. Dartois, Prebiotic chemistry in icy grain mantles in space. An experimental and observational approach. *Chem. Soc. Rev.* **42**, 2173–2185 (2013). Medline doi:10.1039/c2cs35425j

20. Y. S. Kim, R. I. Kaiser, on the formation of amines (RNH_2) and the cyanide anion (CN^-) in electron-irradiated ammonia-hydrocarbon interstellar model ices. *Astrophys. J.* **729**, 68–75 (2011). doi:10.1088/0004-637X/729/1/68

21. L. E. Orgel, Prebiotic chemistry and the origin of the RNA world. *Crit. Rev. Biochem. Mol. Biol.* **39**, 99–123 (2004). Medline doi:10.1080/10409230490460765

22. R. Pascal, L. Boiteau, A. Commeyras, From the prebiotic synthesis of α-amino acids towards a primitive translation apparatus for the synthesis of peptides. *Top. Curr. Chem.* **259**, 69–122 (2005). doi:10.1007/b136707

23. D. Ritson, J. D. Sutherland, Prebiotic synthesis of simple sugars by photoredox systems chemistry. *Nat. Chem.* **4**, 895–899 (2012). Medline doi:10.1038/nchem.1467

24. R. Saladino, C. Crestini, F. Ciciriello, G. Costanzo, E. Di Mauro, Formamide chemistry and the origin of informational polymers. *Chem. Biodivers.* **4**, 694–720 (2007). Medline doi:10.1002/cbdv.200790059

25. C. Giri, F. Goesmann, A. Steele, T. Gautier, H. Steininger, H. Krüger, U. J. Meierhenrich, Competence evaluation of COSAC flight spare model mass spectrometer: In preparation of arrival of Philae lander on comet 67P/Churyumov–Gerasimenko. *Planet. Space Sci.* **106**, 132–141 (2015). doi:10.1016/j.pss.2014.12.017

26. A. Jiménez-Escobar, B. M. Giuliano, G. M. Muñoz Caro, J. Cernicharo, N. Marcelino, Investigation of HNCO isomer formation in ice mantles by UV and thermal processing: An experimental approach. *Astrophys. J.* **788**, 19 (2014). doi:10.1088/0004-637X/788/1/19

27. Y.-K. Kim, M. E. Rudd, Binary-encounter-dipole model for electron-impact ionization. *Phys. Rev. A* **50**, 3954–3967 (1994). Medline doi:10.1103/PhysRevA.50.3954

28. W. Hwang, Y. K. Kim, M. E. Rudd, New model for electron-impact ionization cross sections of molecules. *J. Chem. Phys.* **104**, 2956–2966 (1996). doi:10.1063/1.471116

29. S. G. Lias *et al*., Ion energetic data, in *NIST Chemistry WebBook*, NIST Standard Reference Database Number 69, P. J. Linstrom, W. G. Mallard, Eds. (National Institute of Standards and Technology, Gaithersburg, MD).

30. M. W. Schmidt, K. K. Baldridge, J. A. Boatz, S. T. Elbert, M. S. Gordon, J. H. Jensen, S. Koseki, N. Matsunaga, K. A. Nguyen, S. Su, T. L. Windus, M. Dupuis, J. A. Montgomery, General atomic and molecular electronic structure system. *J. Comput. Chem.* **14**, 1347–1363 (1993). doi:10.1002/jcc.540141112

31. M. S. Gordon, M. W. Schmidt, in *Theory and Applications of Computational Chemistry: The First Forty Years*, C. E. Dykstra, G. Frenking, K. S. Kim, G. E. Scuseria, Eds. (Elsevier, Amsterdam, 2005), pp. 1167–1189.

32. A. G. Harrison, E. G. Jones, S. K. Gupta, G. P. Nagy, Total cross sections for ionization by electron impact. *Can. J. Chem.* **44**, 1967–1973 (1966). doi:10.1139/v66-293